International Journal of Engineering Science 188 (2023) 103866

Contents lists available at ScienceDirect

International Journal of Engineering Science

journal homepage: www.elsevier.com/locate/ijengsci

Analytical solutions of peridynamic equations. Part II: Elastic wave propagation

Ziguang Chen [a,b,*], Xuhao Peng [a], Siavash Jafarzadeh [c,**], Florin Bobaru [c,***]

[a] Department of Engineering Mechanics, School of Aerospace Engineering, Huazhong University of Science and Technology, Wuhan, 430074, China
[b] Hubei Key Laboratory of Engineering Structural Analysis and Safety Assessment, 1037 Luoyu Road, Wuhan, 430074, China
[c] Department of Mechanical and Materials Engineering, University of Nebraska-Lincoln, Lincoln, NE, 68588-0526, United States of America

ARTICLE INFO

Keywords:
Peridynamics
Separation of variables
Series solutions
Analytical solutions
Nonlocal factor
Elasticity

ABSTRACT

We use the separation of variables technique to construct analytical solutions for peridynamic models of dynamic elasticity. We show that, similar to the case of peridynamic models for transient diffusion, infinite series nonlocal solutions for peridynamic elasticity can be obtained directly from the solutions of the corresponding classical model by inserting "peridynamic/nonlocal factors" in the time-exponential part of the solution. The analytical solutions show that wave dispersion, caused by nonlocality, is contained in the horizon-dependent nonlocal factor. We obtain formulas for wave dispersion and group velocities for 1D and 2D peridynamic elastic wave propagation with three commonly-used peridynamic kernels. We observe interesting complexity in nonlocal solutions, generated by nonlocal wave dispersion, and "proportional" to the size of the nonlocal interaction region. Different from the diffusion case, as time goes to infinity, the nonlocal solution for elasticity does not converge to the classical one for a fixed horizon size, meaning that nonlocal effects persist in time. We solve several examples of wave propagation with Dirichlet boundary conditions and smooth or discontinuous initial conditions and compare these analytical solutions with those corresponding to the classical model, which is seen as a particular case of the PD model for horizon equal to zero. Interestingly, we find that in PD solutions, initial discontinuities in space persist at the same location, in time. While most of the analytical solutions we present here are formal, for some of the cases, we are able to prove uniform convergence of the series solutions. This work is the first presentation of a systematic analytical treatment of peridynamic problems in 2D finite domains.

1. Introduction

The peridynamic (PD) theory, introduced by Dr. Silling in 2000 (Silling, 2000), is based on nonlocal interactions between material points in a continuum. In a PD model, the interaction between a material point and its neighbors extends beyond the nearest neighbors, over a region called "the horizon". Given the replacement of the spatial differential operators with an integral one, displacement discontinuities are easily handled in this theory, and with a PD model fracture and damage result naturally from the solution process.

* Corresponding author.
** Corresponding author.
*** Corresponding author.
E-mail addresses: zchen@hust.edu.cn (Z. Chen), sia.jafarzadeh@gmail.com (S. Jafarzadeh), fbobaru2@unl.edu (F. Bobaru).

https://doi.org/10.1016/j.ijengsci.2023.103866
Received 8 March 2021; Received in revised form 11 February 2023; Accepted 25 March 2023
Available online 31 March 2023

The relation between PD and conventional/classical (PDE-based) formulations for elasticity, as well as convergence of numerical schemes for approximating solutions to PD models, have been analyzed in, for example (Seleson, 2014; Silling & Askari, 2005; Silling & Lehoucq, 2008).

While tough problems related to fracture become easy in PD, finding analytical solutions for the integro-differential peridynamic formulations seems more complicated than finding analytical solutions for the corresponding classical models of elastodynamics. A number of analytical solutions have been reported for PD models, but all appear to be limited to infinite domains: static and dynamic response has been studied in Mikata (2012); Silling et al. (2003); Wang et al. (2017); Weckner and Abeyaratne (2005), solitary waves in Silling (2016), and defect propagation by Wang and Abeyaratne (2018). Only a few of analytical solutions to PD elastodynamic problems posed in 1D finite domains have been reported (Chen et al., 2018), and none in 2D or 3D finite domains.

In Part I of this work (Chen et al., 2022), we reported a way of obtaining analytical solutions of peridynamic equations for diffusion problems (in 1D and 2D, and easily extendable to 3D) based on existing series solutions of the corresponding classical formulation of the problem. The PD analytical solutions, derived from the corresponding infinite series classical solutions, insert a nonlocal factor, named here the "PD (nonlocal) factor", in the time-dependent term of the local solution. The nonlocal factors depend on the horizon size and converge to value one as the horizon size goes to zero, recovering the classical form of the solution for the corresponding partial-differential equations. In Part I of this work, we showed that, at time goes to infinity, the nonlocal solution converges to the classical one, for a fixed horizon size.

In this paper, we follow the same approach used in Part I for PD diffusion problems (Chen et al., 2022), and use the method of separation of variables to find analytical solutions of PD models for dynamic elasticity corresponding to classical models for which analytical solutions can be found via separation of variables. Our methodology allows to directly write analytical solutions for PD models in elasticity based on series solutions of the corresponding classical model. These PD solutions satisfy the initial and local boundary conditions posed for the classical formulations of elasticity problems.

2. Analytical solutions for 1D peridynamic models of dynamic elasticity

In the following we adopt the method of separation of variables for classical wave equation (Greenberg, 1988) to arrive at analytical solutions for PD elasticity.

2.1. Separation of variables for 1D peridynamic wave equation

The 1D linear elasticity (wave) PD equation can be expressed as:

$$\frac{\partial^2 u(x,t)}{\partial t^2} = v^2 \mathscr{L}_\delta u(x,t) \tag{1}$$

where $u(x,t)$ is the displacement field which is a function of position x and time t, and $v = \sqrt{\frac{E}{\rho}}$ (E is the Young modulus, ρ is the mass density) is the wave speed. $\mathscr{L}_\delta$ denotes the PD Laplacian operator, defined by:

$$\mathscr{L}_\delta u(x,t) = \int_{\mathrm{H}_x} \mu(|\widehat{x}-x|)[u(\widehat{x},t)-u(x,t)]\mathrm{d}\widehat{x} \tag{2}$$

an integral over a finite size neighborhood of x: H_x, which, in 1D, is a line segment centered at x of length 2δ. We refer to δ as the *horizon size* or simply the horizon. μ is the *kernel* function with $\mu = \mu(|\xi|)$, with support H_x ($\mu(|\xi|) = 0$ for $|\xi| > \delta$, where $\xi = \widehat{x} - x$).

Inspired by the derivation of analytical solutions for problems described by partial differential equations (PDEs), we use the method of *separation of variables* to find analytical solutions for Eq. (1), subjected to initial and (local) boundary conditions. We seek, therefore, a solution to Eq. (1) in the form of a product:

$$u(x,t) = X(x)\mathrm{T}(t). \tag{3}$$

Substituting Eq. (3) into Eq. (1) gives:

$$\mathrm{X}(x)\mathrm{T}''(t) = v^2 \mathrm{T}(t)\mathscr{L}_\delta \mathrm{X}(x) \tag{4}$$

where the double-prime denotes second order ordinary differentiation with respect to t. Dividing Eq. (4) by $\mathrm{X}(x)\mathrm{T}(t)$ leads to:

$$\frac{1}{v^2}\frac{\mathrm{T}(t)''}{\mathrm{T}(t)} = \frac{\mathscr{L}_\delta \mathrm{X}(x)}{\mathrm{X}(x)} \tag{5}$$

Since the left-hand side of Eq. (5) is a function of t only, and the right-hand side is a function of x only, we conclude that:

$$\frac{1}{v^2}\frac{\mathrm{T}(t)''}{\mathrm{T}(t)} = \frac{\mathscr{L}_\delta \mathrm{X}(x)}{\mathrm{X}(x)} = \text{constant in } x \text{ and } t \ = \psi^\delta \tag{6}$$

where the superscript δ in ψ^δ denotes the dependency on δ. As a result, a solution for the integro-differential Eq. (1) must be a solution to the following pair of equations, an ordinary differential equation (ODE) and an integral equation:

$$\mathrm{T}''(t) - v^2\psi^\delta \mathrm{T}(t) = 0 \tag{7}$$

$$\mathscr{L}_\delta \mathrm{X}(x) - \psi^\delta \mathrm{X}(x) = 0 \tag{8}$$

The general solution for the ODE Eq. (7) is:

$$\mathrm{T}(t) = \begin{cases} Dt + E & , \text{ if } \psi^\delta = 0 \\ K\sin(v\sqrt{-\psi^\delta}\, t) + L\cos(v\sqrt{-\psi^\delta}\, t) & , \text{ if } \psi^\delta \neq 0 \end{cases} \tag{9}$$

where D, E, K and L are undetermined constants.

In the case of the integral equation (Eq. (8)), we search for a solution X with a form similar to that obtained when using separation of variables for the corresponding classical (local) elastic waves PDEs. Then ψ^δ is found from imposing that the integral equation (Eq. (8)) is satisfied for this X.

We briefly review the form of the solutions for the 1D linear classical wave equation, the local version of the nonlocal form in Eq. (1):

$$\frac{\partial^2 u(x,t)}{\partial t^2} = v^2 \nabla^2 u(x,t) \tag{10}$$

Separation of variables for Eq. (10), leads to:

$$\mathrm{T}^c(t) = \begin{cases} Dt + E & \psi^c = 0 \\ K\sin(vkt) + L\cos(vkt) & \psi^c \neq 0 \end{cases} \tag{11}$$

$$\mathrm{X}^c(x) = \begin{cases} Gx + H & \psi^c = 0 \\ I\sin kx + J\cos kx & \psi^c \neq 0 \end{cases} \tag{12}$$

where $G, H, I, J,$ and k are undetermined constants, and $\psi^c = -k^2$ (see Appendix A and (Kreyszig, 2017) for derivation details). The superscript c in T^c, X^c, and ψ^c stands for the "classical" solution.

As in the diffusion case, see Chen et al. (2022), $\mathrm{X}(x) = Gx + H$ satisfies Eq. (8) for $\psi^\delta = 0$, while for nonzero ψ^δ, we have:

$$\psi^\delta = \widehat{\mu}_k - \beta^\delta \tag{13}$$

where, $\beta^\delta = \int_{-\delta}^{\delta} \mu(|\xi|)\mathrm{d}\xi$ $\widehat{\mu}_k = \widehat{\mu}\left(\frac{Lk}{2\pi}\right) = \int_{-\infty}^{\infty} \mu(|\xi|)\cos(k\xi)\mathrm{d}\xi$ We then write the "ansatz" solution of Eq. (1), $u(x,t)$, by using superposition:

$$u(x,t) = (Gx+H)(Dt+E) + (I\sin kx + J\cos kx)(K\sin(v\sqrt{-\psi^\delta}\, t) + L\cos(v\sqrt{-\psi^\delta}\, t)) \tag{14}$$

We notice that the solution in Eq. (14) is identical to the one for the classical wave problem, with the only difference being the replacement of the $\psi^c = -k^2$ factor with ψ^δ. The same held true for the diffusion case (Chen et al., 2022). Therefore, we can define the same peridynamic ***"nonlocal factor"***,

$$A(k,\delta) = \frac{\psi^\delta}{\psi^c} = \frac{\beta^\delta - \widehat{\mu}_k}{k^2} \tag{15}$$

as in 1D peridynamic diffusion case.

Separation of variables was applied for solving 1D peridynamics in Chen et al. (2018). As in Chen et al. (2018), separation of variables here decouples the integro-differential peridynamic equation into a spatial integral equation (Eq. (8)) and a temporal ordinary differential equation (Eq. (7)). The 1D solution formulation above, however, is more general than the one in Chen et al. (2018). Moreover, the approach we propose here is easily extended to 2D and 3D, and we provide detailed solutions for the 2D case. The authors of (Chen et al., 2018) only cover the 1D case. In addition, we focus our attention on the properties and influence the nonlocal factor has in characterizing nonlocal solutions versus corresponding local ones.

3. Examples of initial and boundary value problems for 1D peridynamic elasticity

First we consider an IBVP (with Dirichlet boundary conditions) in PD elasticity: a bar of length L, with given initial displacement $g(x)$, and velocity $f(x)$ along the bar, and zero displacements imposed at the ends of the bar:

$$\begin{cases} \rho\dfrac{\partial^2 u(x,t)}{\partial t^2} = E\mathscr{L}_\delta u(x,t) \\ u(x,0) = g(x) \text{ and } u_t(x,0) = f(x),\ 0 \le x \le L \\ u(0,t) = u(L,t) = 0,\ t > 0 \end{cases} \tag{16}$$

We further assume that the kernel function (which specifies the PD Laplace operator) has the form (Chen & Bobaru, 2015):

$$\mu(|\xi|) = \begin{cases} \dfrac{(3-n)}{\delta^{(3-n)}} \dfrac{1}{|\xi|^n}, & |\xi| \le \delta \\ 0, & |\xi| > \delta \end{cases}, \text{ with } n = 0, 1, \text{ or } 2. \tag{17}$$

In order to obtain the PD analytical solution for this problem, we first write the solution for the corresponding local problem:

$$\begin{cases} \rho \dfrac{\partial^2 u(x,t)}{\partial t^2} = E\nabla^2 u(x,t) \\ u(x,0) = g(x) \text{ and } u_t(x,0) = f(x), \ 0 \le x \le L \\ u(0,t) = u(L,t) = 0, \ t > 0 \end{cases} \tag{18}$$

The exact solution to this local IBVP can be written as (Kreyszig, 2017):

$$u_c(x,t) = \sum_{m=1}^{\infty} (D_m \cos(v k_m t) + H_m \sin(v k_m t)) \sin k_m x \tag{19}$$

where the wave speed $v = \sqrt{\frac{E}{\rho}}$, and $k_m = \frac{m\pi}{L}$ with m being a positive integer. D_m and H_m are found from the initial conditions:

$$D_m = \frac{2}{L} \int_0^L f(x) \sin(k_m x) \mathrm{d}x \tag{20}$$

$$H_m = \frac{2}{v k_m L} \int_0^L g(x) \sin(k_m x) \mathrm{d}x \tag{21}$$

Note that depending on the boundary conditions, the "wavenumber" k_m takes different forms.
Using the kernel function in Eq. (17) into Eq. (15), we obtain the corresponding PD/nonlocal factor:

$$A(k_m, \delta) = \frac{\psi^\delta}{-k_m^2} = -\frac{\widehat{\mu}_{k_m} - \beta^\delta}{k_m^2} = -\frac{1}{k_m^2} \int_{-\delta}^{\delta} \frac{(3-n)}{\delta^{(3-n)}} \frac{1}{|\xi|^n} [\cos(k_m \xi) - 1] \, \mathrm{d}\xi = -\frac{(3-n)}{(k_m \delta)^2} \int_{-1}^{1} \frac{\cos k_m \delta \xi - 1}{|\xi|^n} \mathrm{d}\xi \tag{22}$$

From Eq. (22) we notice that using kernels given by Eq. (17) leads to $A(k_m, \delta) = A_n(r_m)$ where $r_m = k_m \delta$, and the subscript n refers to the n value for the specific kernel. By replacing k_m with $\sqrt{A_n(r_m)} k_m$ in the classical solution in Eq. (19), we arrive at:

$$u_{\mathrm{pd}}(x,t) = \sum_{m=1}^{\infty} \left(D_m \cos\left(v \sqrt{A_n(r_m)}\, k_m t \right) + H_m \sin\left(v \sqrt{A_n(r_m)}\, k_m t \right) \right) \sin(k_m x) \tag{23}$$

where the nonlocal factor, $A_n(r_m)$, is given in Eq. (22). Since the nonlocal factor only shows up in the time-dependent term in the infinite series, similar to the diffusion case in Part I of this work, the PD Dirichlet boundary conditions are automatically satisfied. The methods described here are applicable to other types of boundary conditions.

3.1. Analytical results for 1D wave dispersion for different PD kernels

In this section we analyze the dispersion properties of the different PD kernels used in this work. From Eq. (23), we obtain the dispersion relation (eigenvalues):

$$\omega_m = v \sqrt{A_n(r_m)} k_m \tag{24}$$

The group velocity is defined as:

$$v_g = \frac{\mathrm{d}\omega_m(k_m)}{\mathrm{d}k_m} \tag{25}$$

Recall that group velocity is the propagation velocity of the envelope of a modulated travelling wave, which is considered as the propagation velocity of information or energy contained in it.

Waves with the negative group velocity are known to exist in optics and in some mechanical cases like layered media, cylindrical shells and cylinders (Tamm et al., 2017).

Substituting Eqs. (28), (29), (31) in Part I of this work (Chen et al., 2022) and Eq. (24) into Eq. (25), we obtain:

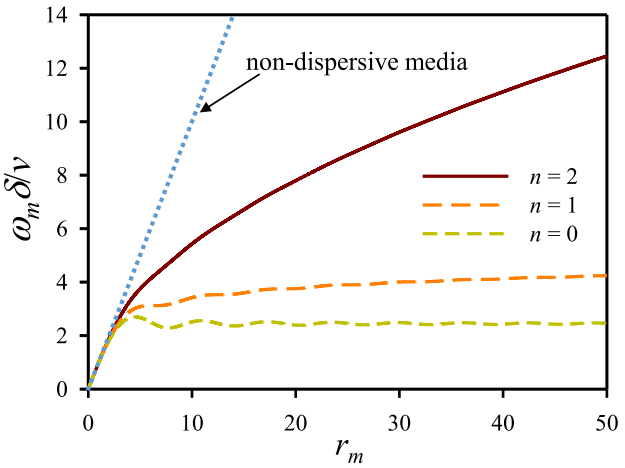

Fig. 1. Dispersion relations for 1D PD dynamic elasticity with different kernels (different n values).

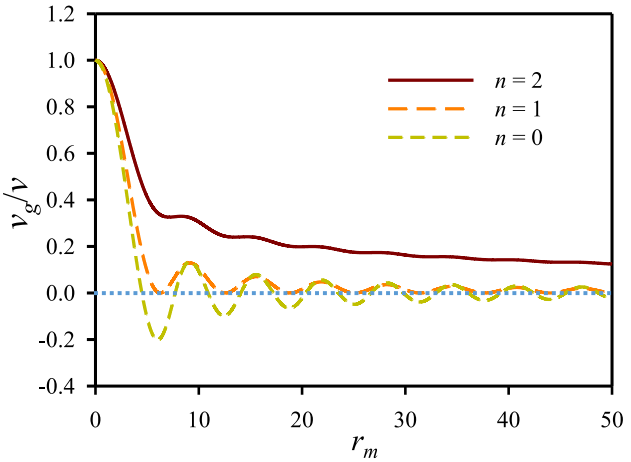

Fig. 2. 1D normalized group velocities ($\frac{v_g}{v}$) as a function of r_m for PD formulations with different kernels (different n values).

$$\frac{v_g}{v} = \begin{cases} \dfrac{3\left(\dfrac{\sin(r_m)}{r_m} - \cos(r_m)\right)}{r_m\sqrt{6\left(1 - \dfrac{\sin(r_m)}{r_m}\right)}}, & n = 0 \\ \dfrac{4(1-\cos(r_m))}{r_m\sqrt{-\mathrm{Ci}(r_m) + \ln(r_m) + \gamma}}, & n = 1 \\ \dfrac{\mathrm{Si}(r_m)}{\sqrt{2r_m\left(\mathrm{Si}(r_m) + \dfrac{\cos(r_m) - 1}{r_m}\right)}}, & n = 2 \end{cases} \tag{26}$$

The non-dimensionalized dispersion curves and non-dimensionalized group velocities are shown in Figs. 1 and 2, respectively. Since $\mathrm{Si}(r_m) > 0$, $1 - \cos(r_m) \geq 0$, and $\frac{\sin(r_m)}{r_m} - \cos(r_m)$ can be smaller than zero, we have: when $n = 2$, the group velocities are always positive; when $n = 1$, the group velocities are always positive or zero; when $n = 0$, the group velocities can be negative for certain r_m. Fig. 2 confirms this observation from Eq. (26). The existence of the negative group velocities in the case of $n = 0$ indicates that PD formulation with $n = 0$ can be used for modeling materials with anomalous dispersion (Mikata, 2012).

3.2. *Example 1: exact solution for a 1D elastic problem with Dirichlet boundary conditions*

In this section, we apply the PD analytical solution for a Gaussian wave propagating along a 1D bar with fixed ends (Chen, Bakenhus

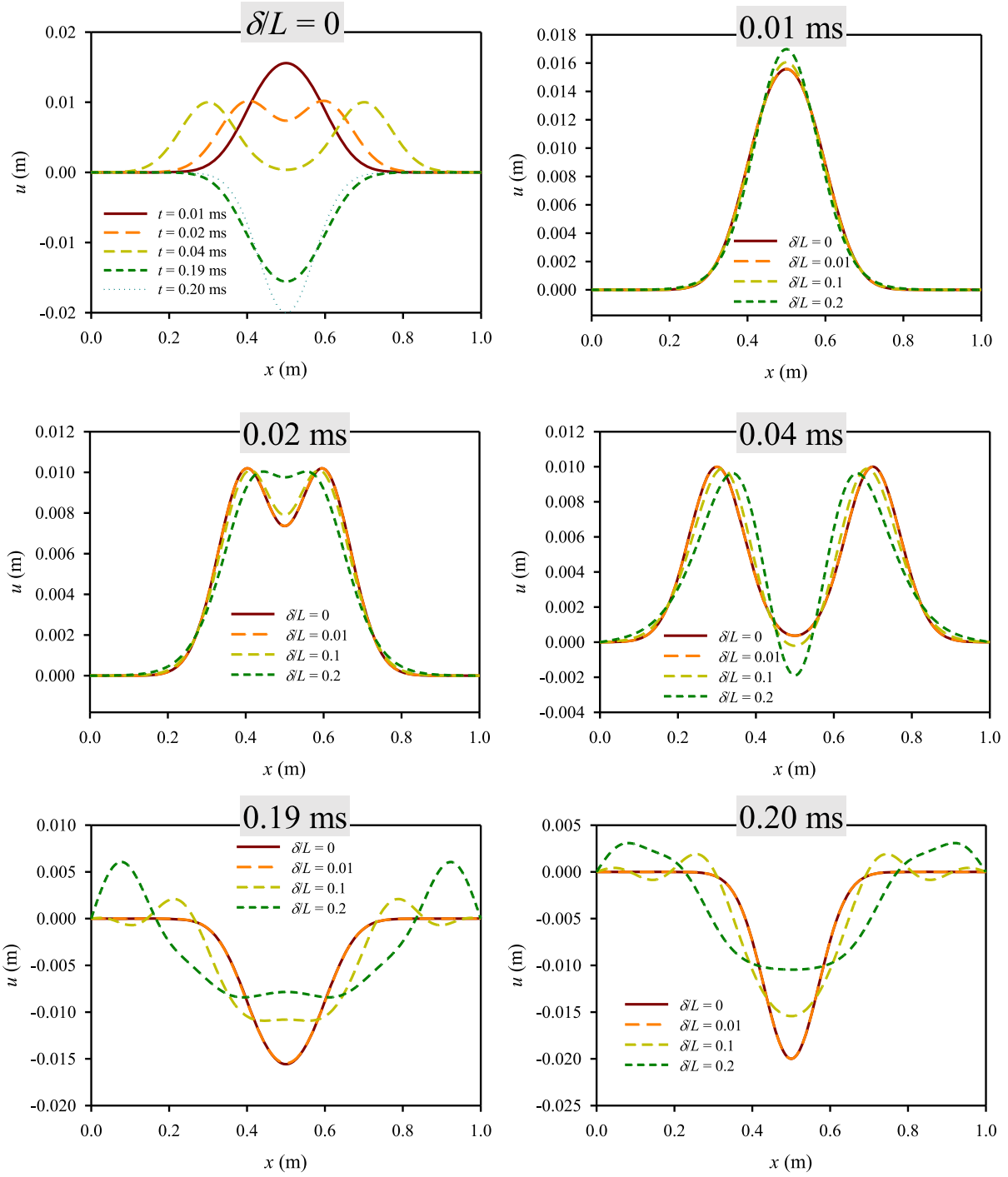

Fig. 3. Example 1: Displacement profiles at time $t = 0.01$ ms, 0.02 ms, 0.04 ms, 0.19 ms and 0.20 ms, from analytical solutions (for $n = 2$) with four different ratios between horizon size and bar length: 0, 0.01, 0.1 and 0.2.

& Bobaru, 2016). A similar example, but with free ends, has been studied with PD in Bobaru et al. (2009). The length of the bar is $L = 1$ m, Young's modulus $E = 200$ GPa, density $\rho = 8000$ kg/m^3. The initial displacement imposed on the elastic bar is a Gaussian of the form $u(x, 0) = 0.02\exp(-100(x - 0.5)^2)$ m. The initial velocity along the bar is $v(x,0) = 0$ m/s. The PD solution as an infinite series is:

$$u(x,t) = \sum_{m=1,\ 3,\ 5\ldots}^{\infty} D_m \cos\left(v\sqrt{A_n(r_m)}\,k_m t\right)\sin(k_m x) \tag{27}$$

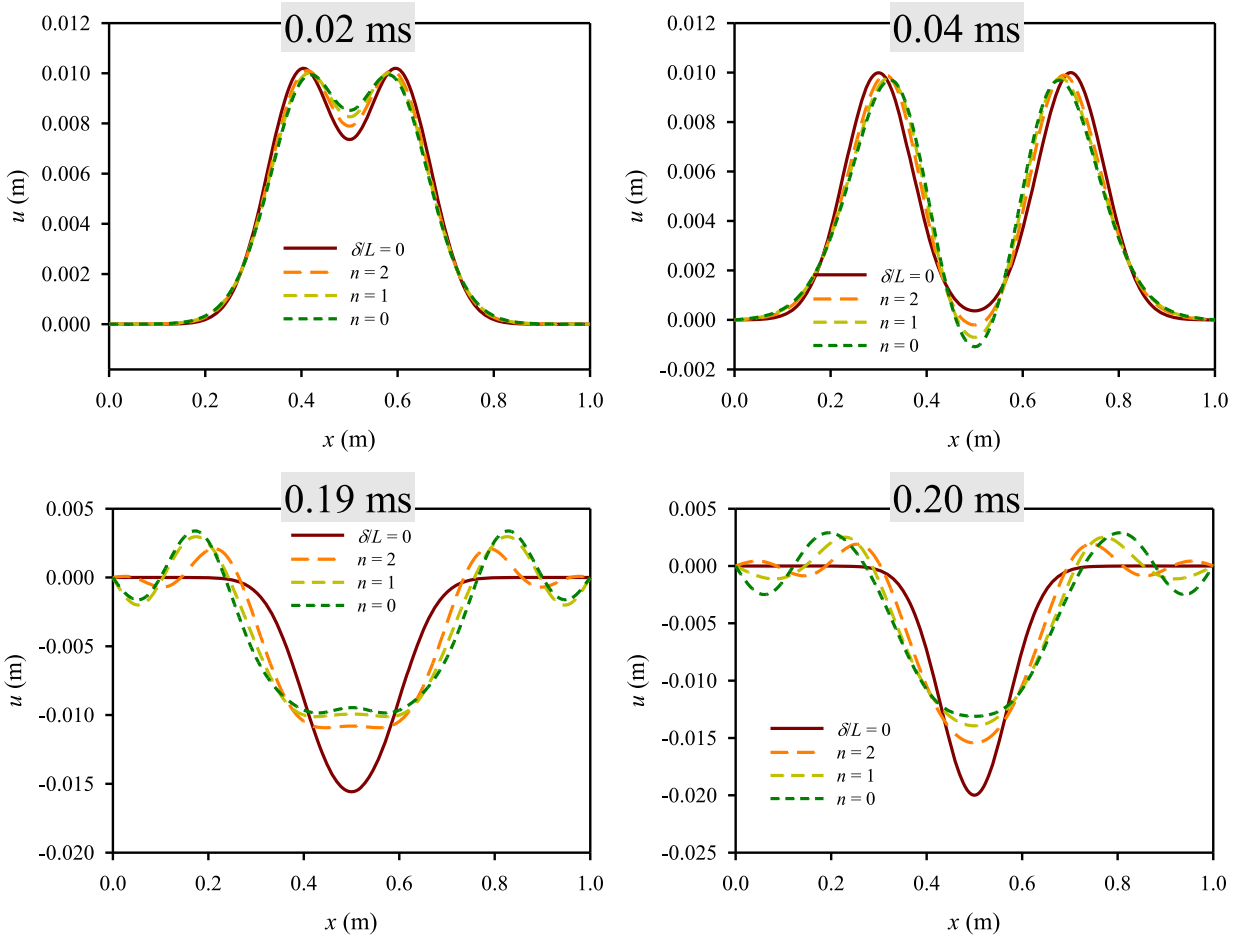

Fig. 4. Example 1: Comparison of solutions from PD formulations with different kernel (different n values). The ratio between horizon size and bar length is 0.1. Classical solution shown by the solid curve.

where,

$$D_m = \left(0.004\sqrt{\pi}\ /\ L\right)\sin\left(\frac{m\pi}{2}\right)\exp\left(-\frac{{k_m}^2}{400}\right) \tag{28}$$

Since $|D_m\cos(v\sqrt{A_n(r_m)}\,k_m t)\sin(k_m x)| \le (0.004\sqrt{\pi}\ /L)\exp\left(-\frac{{k_m}^2}{400}\right)$, and $\sum_{m=1,\,3,\,5\ldots}^{\infty}\exp\left(-\frac{{k_m}^2}{400}\right)$ converges uniformly (satisfying the Weierstrass M-test), the solution in Eq. (27) converges uniformly.

The classical solution (recovered when $\delta = 0$) and the PD solutions for horizon sizes $\delta = 0.01L,\ 0.1L$ and $0.2L$ are plotted, at a number of time instances, in Fig. 3. The first 40 terms of the PD series solutions are used for the plots and videos in Sections 3.2 and 3.3 (see Fig. 15 in Appendix B for the average difference between the PD solutions and corresponding classical solutions). In this figure, solutions are from the PD formulation with $n = 2$ defining its kernel. Fig. 3 shows how wave dispersion enlarges with time, and the larger the horizon size, the higher the effect of wave dispersion.

In Fig. 4, we fix the horizon size to be $0.1L$ (except for the case of the classical solution), and compute results for different n values in the PD kernel. As seen from the dispersion curves in Fig. 1, the PD formulation corresponding to the kernel with $n = 0$, has a stronger nonlocal dispersion effect compared with the other two choices for n; the one with $n = 2$, shows the weakest dispersion.

3.3. Nonlocality-induced complexity

In the previous section, we showed that the nonlocal wave dispersion effect persists in time. In observing the long time behavior of wave propagation, numerical simulations are limited by the stability-requirements on the size of the time step. The analytical solutions obtained in this work, will enable us to compute the wave profile over any time period. In this section, we show that the PD nonlocality leads to highly complex behavior and "random" oscillations. We consider the same example shown in the last section and monitor the displacement (u) at the center point ($x = 0.5$ m) on the elastic bar in time.

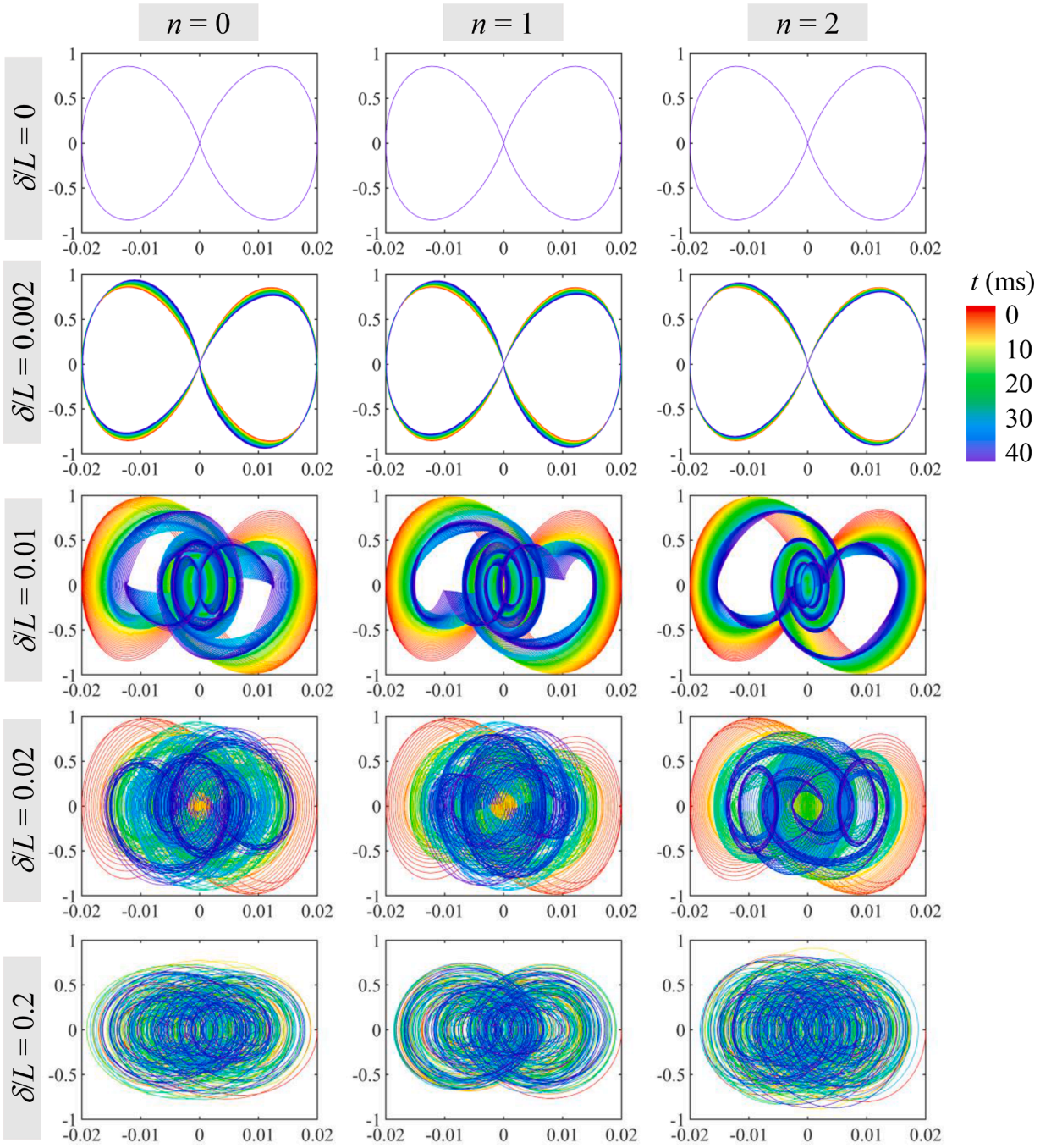

Fig. 5. Phase-plane (velocity versus displacement), for different horizon sizes and the three types of PD kernels. Along the y-axes we have du/dt (m/s) at the center point of the bar ($x = 0.5$ m), while on the x-axes we have the displacement at the center point in m. The color scheme represents the time, from 0 to 40 ms.

For the three types of PD kernels, we use the analytical solution to compute the displacement and velocity at the middle point during the first 40 ms. Fig. 5 gives the phase-plane plots (velocity versus displacement), for different horizon sizes. The results show that wave dispersion, caused by nonlocality, changes the harmonic local oscillations into quasi-periodic behavior, and then to "random"-like complexity. To more intuitively show the phase transition induced by the nonlocal wave dispersion, in Videos 1–4, we present the phase-plane evolution from these analytical PD solutions with $n = 2$. Four different horizon sizes, $0.002L$, $0.01L$, $0.02L$ and $0.2L$, are used for the results seen in Videos 1–4, respectively. Nonlocality-generated complexity, useful in data encryption, has been recently reported in other nonlocal operators, like fractional differential operators (Lizama, Murillo-Arcila & Peris, 2020). The

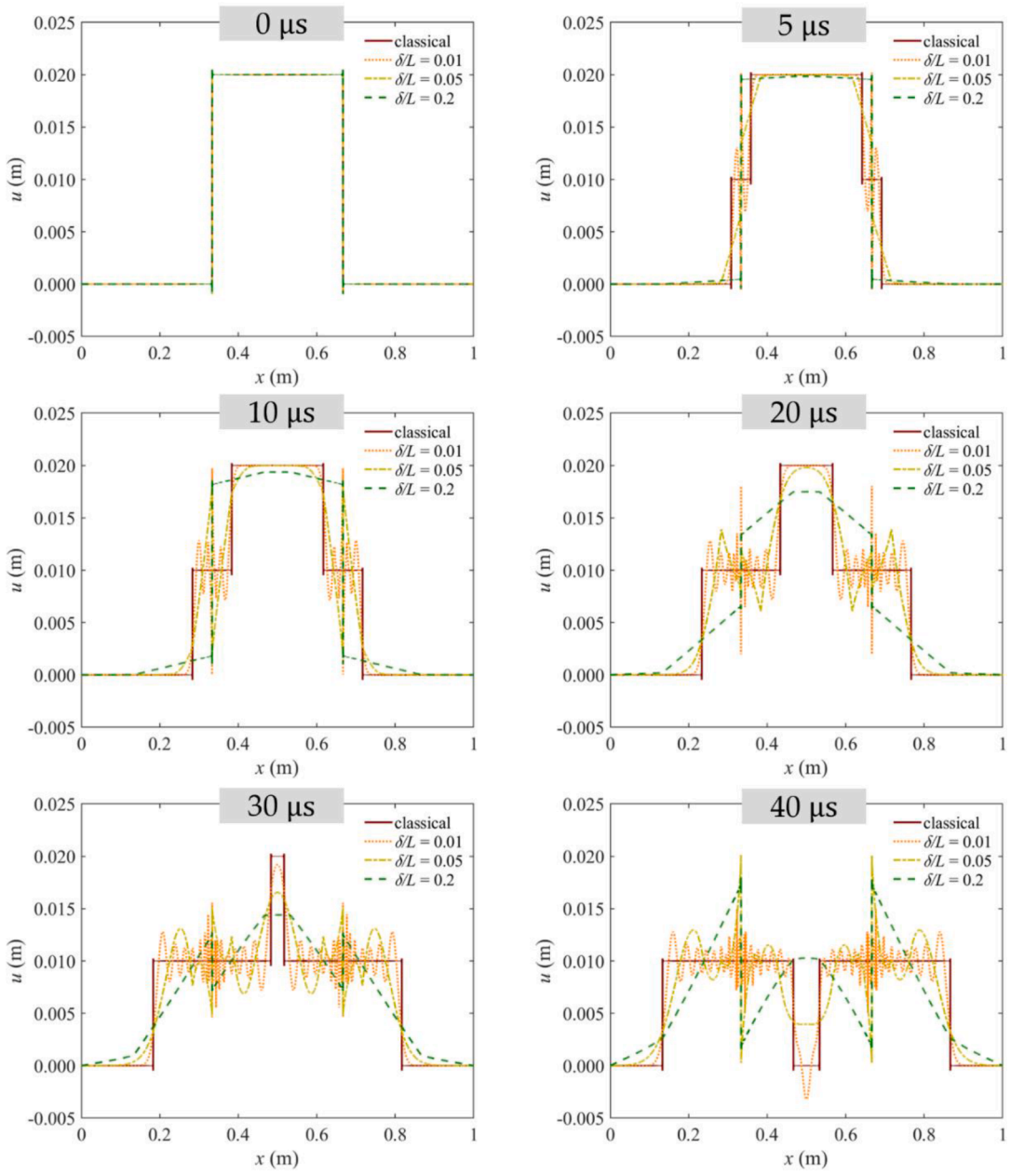

Fig. 6. Example 2: Displacement profiles at time $t = 0$, 5, 10, 20, 30 and 40 μs, from the classical and PD analytical solutions with different horizon size ($\delta = 0.01,\ 0.05,$ and $0.2L$) for the PD kernel with $n = 0$.

"random"-like complex behavior observed here for the first time in PD models will be further investigated in the future.

3.4. Example 2: exact solution for a 1D elastic problem with an initial discontinuous displacement

The example considered in the last two subsections had a smooth initial displacement. To check the ability of the developed analytical PD method to solve problems with discontinuities, in the following two subsections we consider the following non-smooth initial conditions: (1) 1D propagation of a square wave, and (2) a 1D elastic problem with initial discontinuous velocity (a similar case was considered in Weckner and Abeyaratne (2005), but in the infinite domain) in Section 3.5. In these two examples, the domain, material properties and boundary conditions are the same as in Example 1.

A square wave initial displacement is imposed on the elastic bar, with $u(x,0) = 0.02$ m for $x \in (L/3, 2L/3)$ and zero elsewhere. The initial velocity is $v(x,0) = 0$ m/s. Both ends of the bar are subjected to the Dirichlet boundary conditions. The infinite series analytical PD solution for these conditions is (see Eq. (23)):

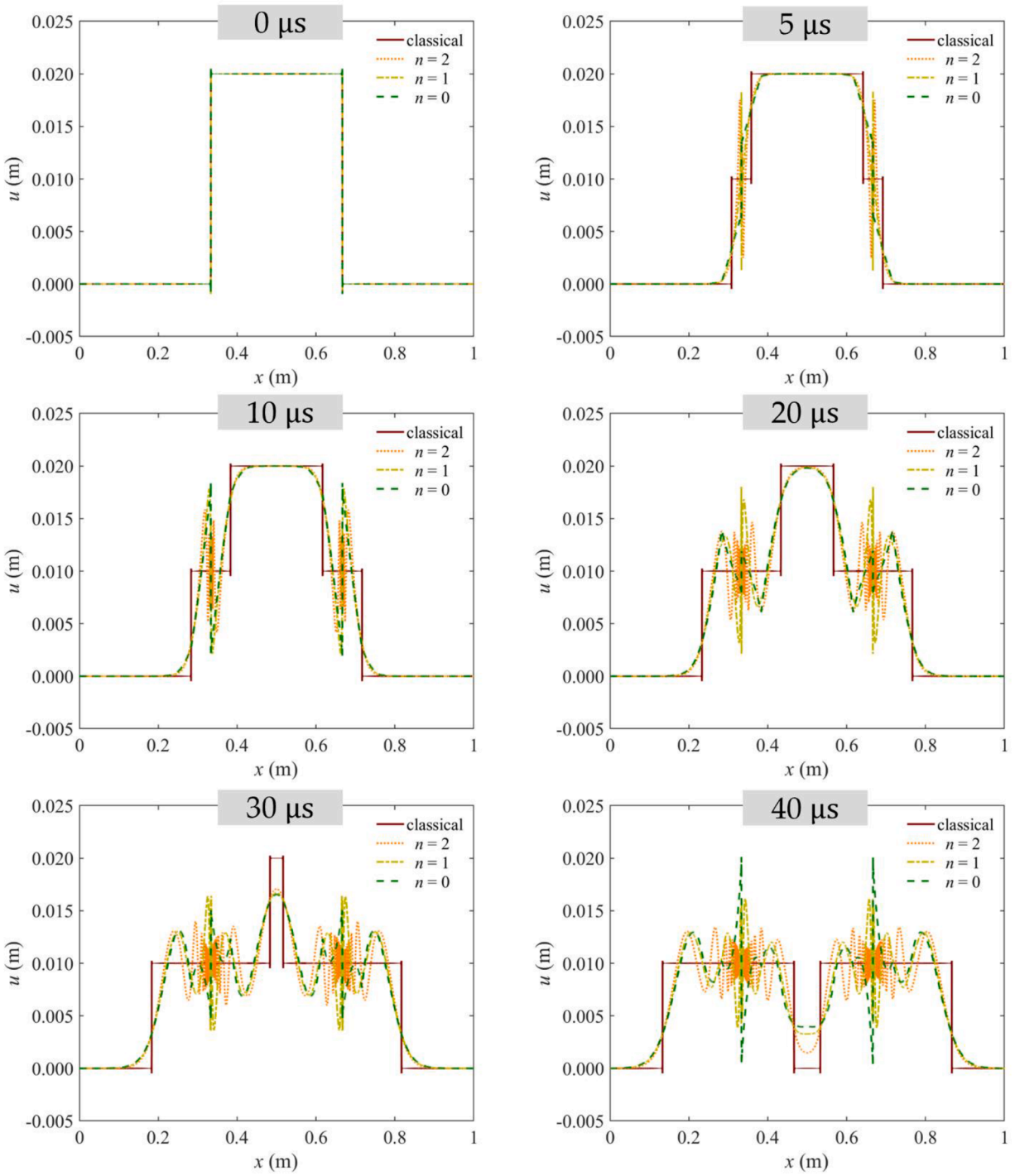

Fig. 7. Example 2: Displacement profiles at time $t = 0$, 5, 10, 20, 30 and 40 μs, from the classical and analytical solutions with different kernel functions ($n = 0,\ 1,\ 2$) for $\delta = 0.05L$.

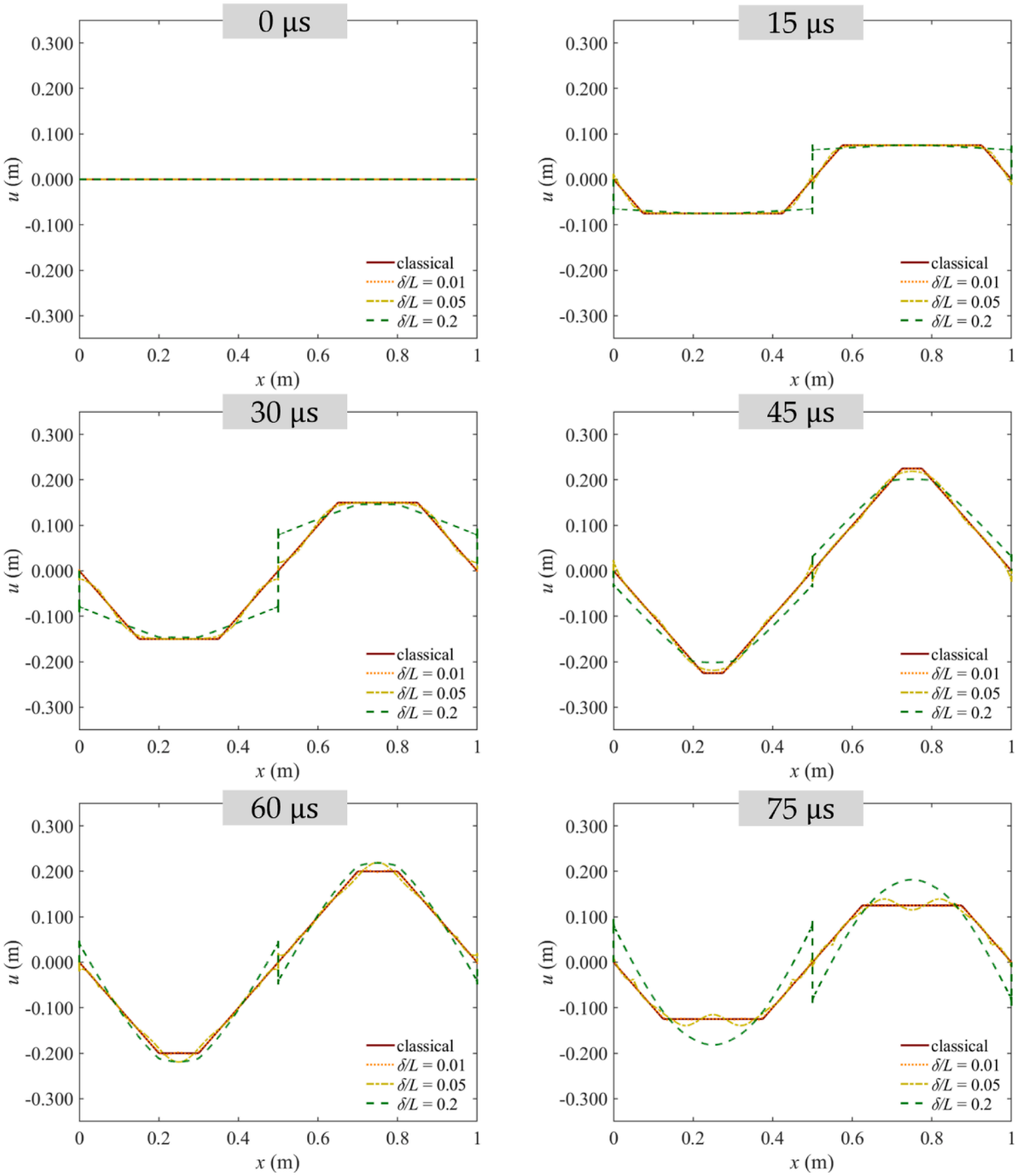

Fig. 8. Example 3: Displacement profiles at times $t = 0$, 15, 30, 45, 60 and 75 μs, from the classical and PD analytical solutions with different horizon size ($\delta = 0.01,\ 0.05,$ and $0.2L$) for the PD kernel with $n = 0$.

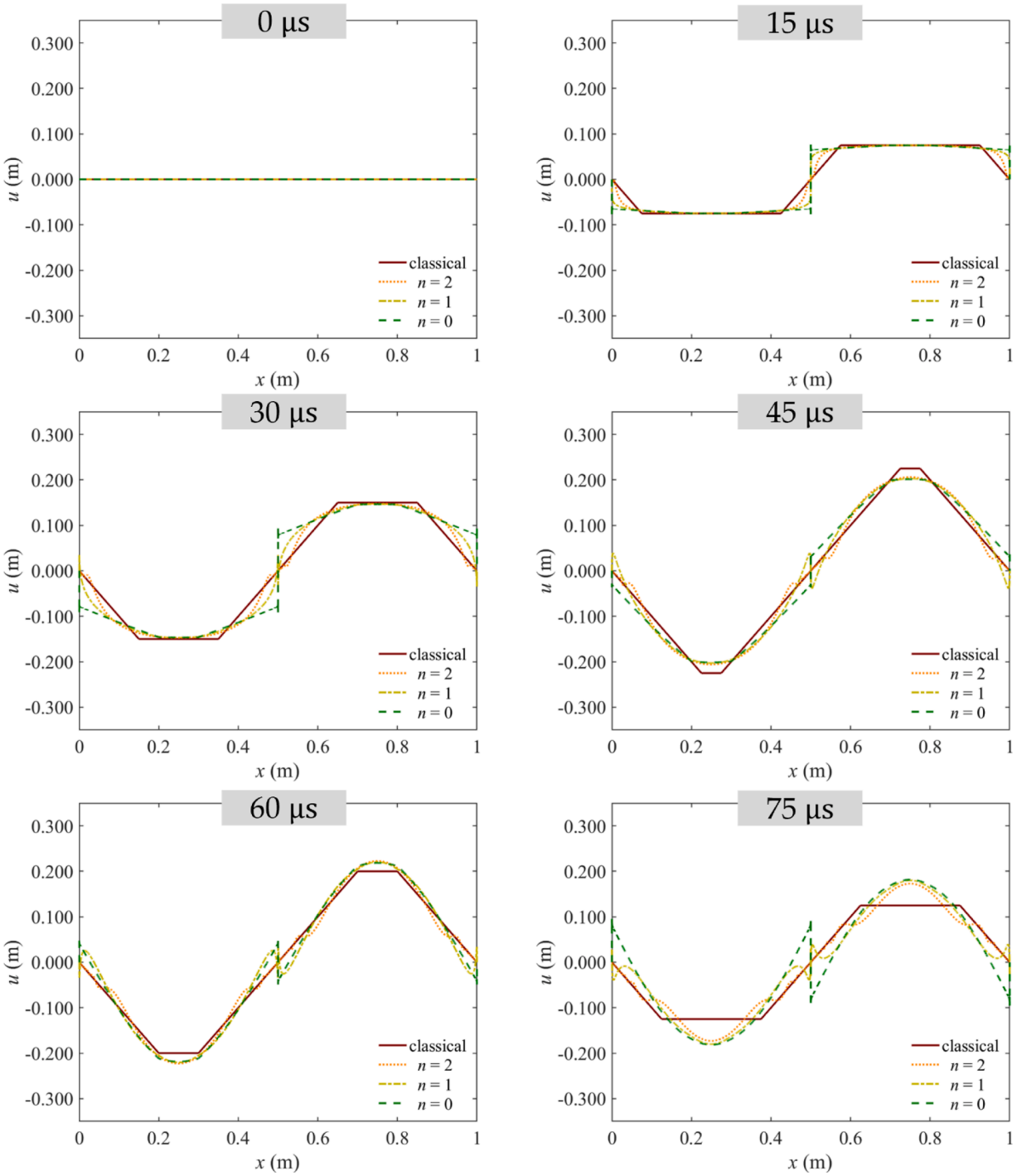

Fig. 9. Example 3: Displacement profiles at times $t = 0$, 15, 30, 45, 60 and 75 μs, from the classical and PD analytical solutions with different kernel functions ($n = 0,\ 1,\ 2$) for $\delta = 0.2L$.

$$u(x,t) = \sum_{m=1,2,3\ldots} D_m \sin\left(\frac{m\pi x}{L}\right)\cos\left(v\sqrt{A_n(r_m)}\,k_m t\right) \tag{29}$$

where,

$$D_m = \frac{0.04}{m\pi}\left(\cos\left(\frac{m\pi}{3}\right) - \cos\left(\frac{2m\pi}{3}\right)\right) \tag{30}$$

Fig. 6 and Video 5 (with the same legend as the one in Fig. 6) show displacement evolution for the classical and corresponding PD analytical solutions with different horizon sizes ($\delta = 0.01L,\ 0.05L,\ 0.2L$) and the PD kernel with $n = 0$. The first 10,000 terms of the PD series solutions are used for the plots and videos in Sections 3.4 and 3.5. The snapshots in Fig. 6 show how displacements vary in time (see Fig. 16 in Appendix B for the average difference between the PD solutions and corresponding classical solutions). A Gibbs type phenomenon is seen around the initial points of discontinuity. The analytical classical solution maintains the shape of the square wave at all times, while the PD solutions are modified by the nonlocality-induced wave dispersion, which is more pronounced the larger the horizon size. Another feature of the PD solutions is the presence of displacement jumps/oscillations at the initial locations of discontinuities, which persist in time. As the horizon size decreases, the oscillation frequency at these locations gets higher. For a small horizon size, e.g., $\delta = 0.01L$, fluctuations are dramatic, while the overall displacement profile of the nonlocal solutions roughly tracks the shape of the classical square wave as it propagates. The classical solution and the PD solution for horizon size $\delta = 0.05L$ with different PD kernels, $n = 0,\ 1,\ 2$, are plotted in Fig. 7. The oscillations characteristics vary with the chosen kernel functions, which the case with $n = 0$, showing the higher jumps, and the $n = 2$ case showing smaller amplitude but higher frequency. This is expected given the more localized behavior implied by the latter versus the former.

3.5. Example 3: exact solution for a 1D elastic problem with a discontinuous initial velocity

In this section, we consider a problem with a discontinuous initial velocity. The initial displacement of this bar is $u(x,0) = 0$, and the initial velocity is $v(x,0) = -v$ for $x < L/2$ and $v(x,0) = v$ for $x > L/2$. Both ends of the bar are subjected to the Dirichlet boundary conditions. This discontinuous problem has been studied for the case of the infinite bar in Weckner and Abeyaratne (2005). The infinite series analytical PD solution for our finite domain BVP is (see Eq. (23)):

$$u(x,t) = \sum_{m=1,2,3\ldots} D_m \sin\left(\frac{m\pi x}{L}\right)\cos\left(v\sqrt{A_n(r_m)}\,k_m t\right) \tag{31}$$

where,

$$D_m = \frac{8}{m\pi k_m \sqrt{A_n(r_m)}}\cos\left(\frac{m\pi}{2}\right)\sin^2\left(\frac{m\pi}{4}\right) \tag{32}$$

The evolution of displacement profiles for the classical and PD analytical solutions (for $n = 0$) with different horizon sizes are shown in Fig. 8 and Video 6 (with the same legend as the one in Fig. 8). In the classical solution, the displacement is continuous through the bar, but the strain contains traveling discontinuities (the spatial derivative of the displacement is not continuous). The displacement fields of the PD nonlocal solutions appear to feature a persistent discontinuity at the middle of the bar, where the initial velocity discontinuity was located. This persistent discontinuity in the PD displacement profile was also observed for the case of infinite bar solved in Weckner and Abeyaratne (2005). The magnitude of displacement jump decreases as the horizon size decreases.

Fig. 9 shows the displacement evolution for classical and PD analytical solutions with different kernel function ($n = 0,\ 1,\ 2$) for the particular horizon size $\delta = 0.2L$. The jump discontinuity in displacements at $x = 0.5$ m (middle of the bar) can be observed for the kernel with $n = 0$ and 1, however, it is barely visible for $n = 2$.

4. Analytical solutions for 2D peridynamic elasticity

In this section, we extend the approach introduced in the previous sections to construct analytical solutions for 2D PD models of linear elastic vibrations of a taut membrane. Extensions to 3D problems would follow a similar pathway.

The PD wave equation for elastic vibrations in a 2D membrane can be expressed as:

$$\frac{\partial^2 u(x,t)}{\partial^2 t} = v^2 \mathscr{L}_\delta u(x,t) \tag{33}$$

where $u(x,t)$ is the deflection of the membrane (the out-of-plane displacement) at location x and time t. $v^2 = \sqrt{\frac{\widetilde{T}}{\rho}}$, and $\widetilde{T}$ is the tension per unit length. ρ in this 2D case is the mass of the undeflected membrane per unit area. $\widetilde{T}$ is the same at all points and does not change during the motion (Kreyszig, 2017), and together with the density ρ are assumed to be given here. The PD Laplacian operator in 2D is:

$$\mathscr{L}_\delta u(x,t) = \int_{\mathrm{H}_x} \mu(|\widehat{x} - x|)[u(\widehat{x},t) - u(x,t)]\mathrm{d}V_{\widehat{x}} \tag{34}$$

which is the area/volume integral over H_x. Boldfaced letters denote vector-valued quantities, e.g. $x = \begin{Bmatrix} x \\ y \end{Bmatrix}$ is the position vector in 2D. The neighborhood H_x in 2D, is a disk centered at x with the radius δ. $\mathrm{d}V_{\widehat{x}}$ is the volume of node $\widehat{x}$ covered by the horizon of node x. μ is the *kernel* function with $\mu = \mu(|\xi|)$, that has the support H_x, therefore $\mu(|\xi|) = 0$ for $|\xi| > \delta$, where $\xi = \widehat{x} - x$ is the bond vector.

Following the method of separation of variables in 2D, we seek a solution of the form:

$$u(x,y,t) = S(x,y)\mathrm{T}(t) = X(x)\mathrm{Y}(y)\mathrm{T}(t) \tag{35}$$

Substituting Eq. (35) into Eq. (33) gives:

$$\mathrm{S}(x,y)\mathrm{T}''(t) = v^2\mathrm{T}(t)\mathscr{L}_\delta \mathrm{S}(x,y) \tag{36}$$

and diving Eq. (36) by ST yields:

$$\frac{1}{v^2}\frac{\mathrm{T}''(t)}{\mathrm{T}(t)} = \frac{\mathscr{L}_\delta \mathrm{S}(x,y)}{\mathrm{S}(x,y)} = \text{constant in } x,y,t \text{ (depends on } \delta) = \psi^\delta \tag{37}$$

As a result, the solution to the integro-differential equation Eq. (33) is the solution to the following pair of equations, an ODE and an integral equation:

$$\mathrm{T}''(t) - v^2\psi^\delta \mathrm{T}(t) = 0 \tag{38}$$

$$\mathscr{L}_\delta \mathrm{S}(x,y) - \psi^\delta \mathrm{S}(x,y) = 0 \tag{39}$$

The ODE in Eq. (38) is identical to that from the 1D case, yielding solution for T as given in Eq. (23).

For the integral equation Eq. (39), we choose $\mathrm{S}(x,y)$ to be the same as the spatial solutions obtained when using separation of variables for the corresponding classical (local) wave PDE (see Appendix A). Then ψ^δ is found from requiring that Eq. (39) is satisfied for this $\mathrm{S}(x,y)$.

For the 2D classical wave equation, separation of variables leads to the following formal solutions (see Appendix A):

$$\mathrm{T}^c(t) = \begin{cases} a_1 t + a_2 & \psi^c = 0 \\ a_3 \sin\left(v\sqrt{-\psi^c}\, t\right) + a_4 \cos\left(v\sqrt{-\psi^c}\, t\right) & \psi^c \neq 0 \end{cases} \tag{40}$$

$$\mathrm{S}^c(x,y) = \mathrm{X}^c(x)\mathrm{Y}^c(y) = \begin{cases} (a_5 + a_6 x)(a_7 + a_8 y) & \psi^c = 0 \\ (a_9 \sin k_1 x + a_{10}\cos k_1 x)(a_{11}\sin k_2 y + a_{12}\cos k_2 y) & \psi^c \neq 0 \;\&\; k_1 \neq 0 \;\&\; k_2 \neq 0 \\ (a_7 + a_8 y)(a_9 \sin k_1 x + a_{10}\cos k_1 x) & \psi^c \neq 0 \;\&\; k_1 \neq 0 \;\&\; k_2 = 0 \\ (a_5 + a_6 x)(a_{11}\sin k_2 y + a_{12}\cos k_2 y) & \psi^c \neq 0 \;\&\; k_1 = 0 \;\&\; k_2 \neq 0 \end{cases} \tag{41}$$

where $a_1, a_2, \ldots, a_{12}$, and k_1 and k_2 are constants, and $\psi^c = -(k_1^2 + k_2^2)$.

As shown in Part I of this work, $\mathrm{S}(x,y) = (a_5 + a_6 x)(a_7 + a_8 y)$ satisfy the integral equation Eq. (39) for $\psi^\delta = 0$, and for nonzero ψ^δ, we have (see for details Chen et al. (2022)):

$$\psi^\delta = 2\pi\widehat{\mu}_k - \beta^\delta \tag{42}$$

where, $\widehat{\mu}_k = \int_0^\infty \mu(w) w J_0\left(\sqrt{k_1^2 + k_2^2}\, w\right) \mathrm{d}w$ is the Hankel transform of order zero for μ evaluated at $\sqrt{k_1^2 + k_2^2} = \sqrt{-\psi^c}$, and $\beta^\delta = \int_0^{2\pi}\int_0^\delta \mu(w) w \mathrm{d}w\mathrm{d}\varphi$ is the integral of the kernel function. J_0 is the zeroth-order Bessel function of the first kind.

The PD nonlocal factor for 2D wave equation is then:

$$A(k_1,k_2,\delta) = \frac{\psi^\delta}{\psi^c} = \frac{2\pi\widehat{\mu}_k - \beta^\delta}{-\left(k_1^2 + k_2^2\right)} = -2\pi\frac{\delta^4}{r^4}\int_0^r \mu\left(\frac{\delta R}{r}\right) R[J_0(R) - 1]\mathrm{d}R \tag{43}$$

where $r = \sqrt{(k_1\delta)^2 + (k_2\delta)^2} = \delta\sqrt{-\psi^c}$.

One can therefore *use any analytical series solution for the 2D classical (PDE-based) wave IBVP to write the analytical solution for the corresponding 2D nonlocal (PD) wave IBVP* by replacing $\psi^c = -(k_1^2 + k_2^2)$ with $A(k_1,k_2,\delta)\psi^c$ in the time-exponential part of the solution. A similar derivation can be carried out for 3D problems.

Next, we present an example for finding analytical solutions to a 2D PD elasticity IBVP with Dirichlet BCs, and also study the 2D wave dispersion using the analytical solutions of the PD models.

5. An initial and boundary value peridynamic elasticity problem in 2D

Here we find the analytical solution for a particular 2D PD elasticity problem with Dirichlet BCs. We consider 2D elastic wave propagation in a vibrating rectangular PD membrane of length L and height H with clamped BCs, with initial displacement and velocity as follows:

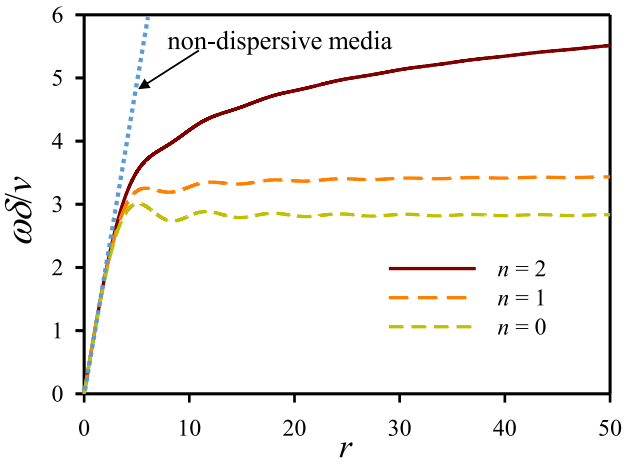

Fig. 10. Dispersion curves for 2D PD elasticity and different kernels (different n values). $r = \sqrt{(k_m\delta)^2 + (k_s\delta)^2}$.

$$\begin{cases} \dfrac{\partial^2 u(x,y,t)}{\partial t^2} = v^2 \mathscr{L}_\delta u(x,y,t) \\ u|_{x=0} = 0, u|_{x=L} = 0, u|_{y=0} = 0, u|_{y=H} = 0 \\ u(x,y,0) = f(x,y) \\ u_t(x,y,0) = g(x,y) \end{cases} \tag{44}$$

with the kernel function that specifies the PD Laplacian operator to be of the form:

$$\mu(|\xi|) = \begin{cases} \dfrac{2(4-n)}{\pi\delta^{(4-n)}} \dfrac{1}{|\xi|^n}, & |\xi| \le \delta \\ 0, & |\xi| > \delta \end{cases}, \text{ and } n = 0, 1, 2 \tag{45}$$

where the kernel function with $n = 2$ (the "constructive kernel") was given in Bobaru and Duangpanya (2012). The kernel functions with $n = 0$, 1 are can be derived by following the same process as shown in Bobaru and Duangpanya (2012).

To obtain the analytical solution, we first find the solution to the classical wave equation subjected to the same boundary and initial conditions. This is (see (Greenberg, 1988)):

$$u(x,y,t) = \sum_{m=1}^{\infty}\sum_{s=1}^{\infty}\left(B_{ms}\cos(\lambda_{ms}t) + B^*_{ms}\sin(\lambda_{ms}t)\right)\sin(k_m x)\sin(k_s y) \tag{46}$$

where $k_m = \frac{m\pi}{L}$, $k_s = \frac{s\pi}{H}$, $\lambda_{ms} = v\sqrt{k_m{}^2 + k_s{}^2}$, and,

$$B_{ms} = \frac{4}{LH}\int_0^H\int_0^L f(x,y)\sin(k_m x)\sin(k_s y)\mathrm{d}x\mathrm{d}y \tag{47}$$

$$B^*_{ms} = \frac{4}{LH\lambda_{ms}}\int_0^H\int_0^L g(x,y)\sin(k_m x)\sin(k_s y)\mathrm{d}x\mathrm{d}y \tag{48}$$

m and s are positive integers.

We then compute the PD nonlocal factor from Eq. (43) for the kernel type in Eq. (45):

$$A_n(k_m,k_s,\delta) = -2\pi\frac{\delta^4}{r^4}\frac{2(4-n)}{\pi\delta^{(4-n)}}\int_0^r \frac{1}{\left(\frac{\delta R}{r}\right)^n} R[J_0(R)-1]\mathrm{d}R = -\frac{4(4-n)}{r^{(4-n)}}\int_0^r \frac{J_0(R)-1}{R^{n-1}}\mathrm{d}R \tag{49}$$

where, $r = r(m,s) = \sqrt{(k_m\delta)^2 + (k_s\delta)^2}$, and J_0 is the zeroth-order Bessel function of the first kind. Similar to the 1D case, we observe that with the kernels of the form in Eq. (45), the PD analytical solution is obtained from the classical solution by replacing $-(k_m{}^2 + k_s{}^2)$ with $-A(k_m,k_s,\delta)(k_m{}^2 + k_s{}^2)$:

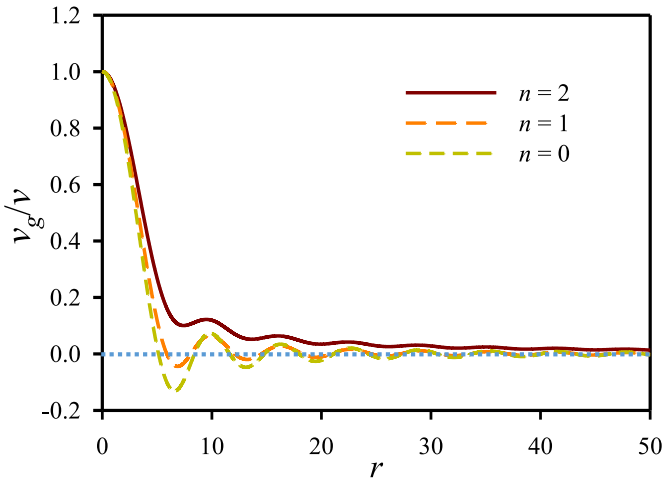

Fig. 11. The normalized group velocities ($\frac{v_g}{v}$) as a function of $r = \sqrt{(k_m\delta)^2 + (k_s\delta)^2}$ for the analytical 2D PD solutions for different kernels (different n values).

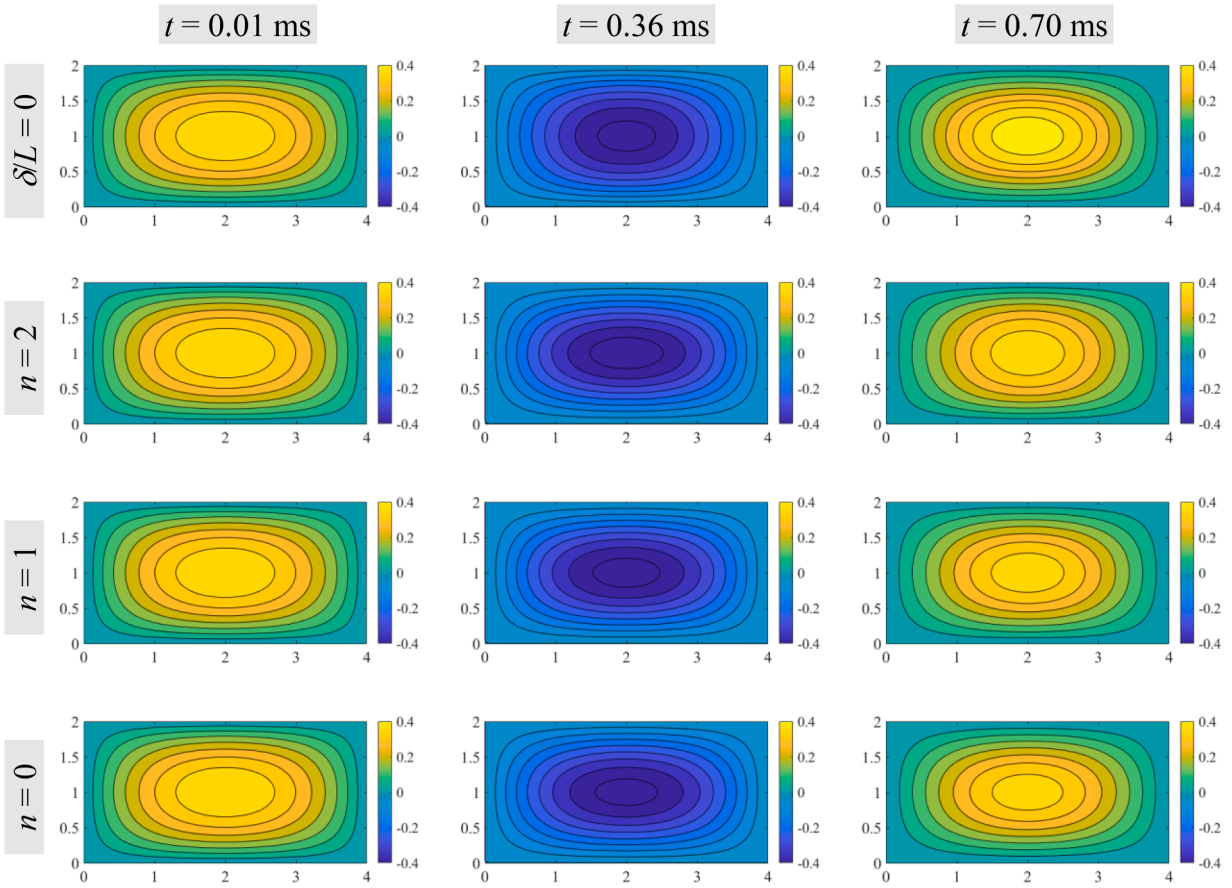

Fig. 12. Example 4: displacement profiles at times $t = 0.01$, 0.36 and 0.70 ms, for the classical solutions and PD solutions with horizon size $0.5H$ and different kernels.

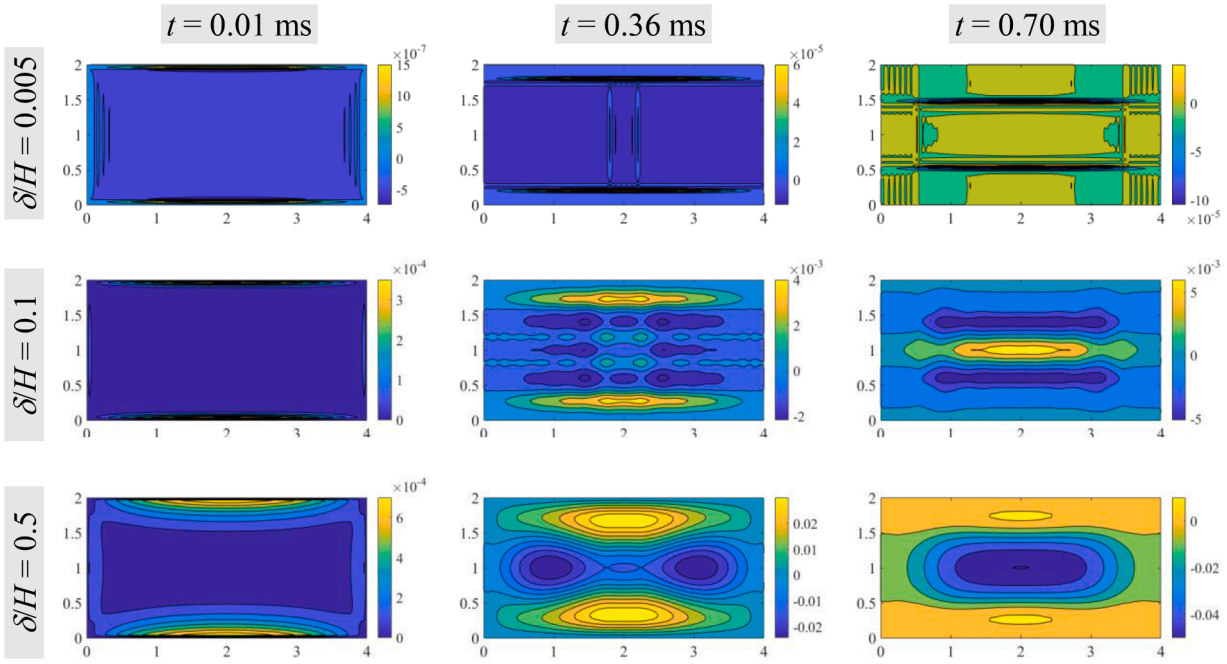

Fig. 13. Example 4: contour plots of the differences in displacements between PD and classical solutions at times: $t = 0.01$, 0.36 and 0.70 ms, with horizon sizes: $0.005H$, $0.1H$ and $0.5H$. PD formulation is for $n = 2$.

$$u_{\mathrm{pd}}(x,y,t) = \sum_{s=1}^{\infty}\sum_{m=1}^{\infty}\left(B_{ms}\cos\left(\lambda_{ms}\sqrt{A_n(r)}\,t\right) + B^{*}_{ms}\sin\left(\lambda_{ms}\sqrt{A_n(r)}\,t\right)\right)\sin(k_m x)\sin(k_s y) \tag{50}$$

where $r = \sqrt{(k_m\delta)^2 + (k_s\delta)^2}$, $k_m = \frac{m\pi}{L}$, and $k_s = \frac{s\pi}{H}$. $A_n(r)$ is given in Eq. (49). Since the nonlocal factor is only involved in the time-related term in the infinite series, similar as the 2D diffusion case, the PD boundary conditions are automatically satisfied.

5.1. Wave dispersion in 2D PD models

From Eq. (50), we obtain the 2D dispersion relation (eigenvalues):

$$\omega\left(\sqrt{{k_m}^2 + {k_s}^2}\right) = \lambda_{ms}\sqrt{A_n(r)} \tag{51}$$

The 2D group velocity is defined as:

$$v_g = \frac{\mathrm{d}\omega_m(r)}{\mathrm{d}\sqrt{{k_m}^2 + {k_s}^2}} = v\frac{\mathrm{d}\left(r\sqrt{A_n(r)}\right)}{\mathrm{d}r} \tag{52}$$

Substituting Eq. (49) and Eq. (51) into Eq. (52), we obtain:

$$\frac{v_g}{v} = \frac{n-2}{2}\sqrt{A_n(r)} - \frac{2(4-n)}{r^2\sqrt{A_n(r)}}(J_0(r) - 1) \tag{53}$$

where J_0 is the zeroth-order Bessel function of the first kind, and $A_n(r)$ is given in Eq. (49).

The 2D non-dimensionalized dispersion curves and non-dimensionalized group velocities are shown in Fig. 10 and Fig. 11, respectively. Fig. 11 shows that when $n = 2$, the group velocities are always positive; when $n = 0$ or 1, the group velocities can be negative for certain values of $\sqrt{(k_m\delta)^2 + (k_s\delta)^2}$.

5.2. Example 4: solution for a particular 2D membrane vibration problem with Dirichlet boundary conditions

In this section, we apply the analytical solution (Eq. (50)) to consider vibration in a rectangular membrane of sides $L = 4$ m and $H = 2$ m. We take $v = 5000$ m/s. The initial velocity is $u_t(x,y,0) = 0$ and the initial displacement is $u(x,y,0) = 0.1(4x - x^2)(2y - y^2)$(Kreyszig, 2017). The analytical PD solution can be written in infinite series form as follow:

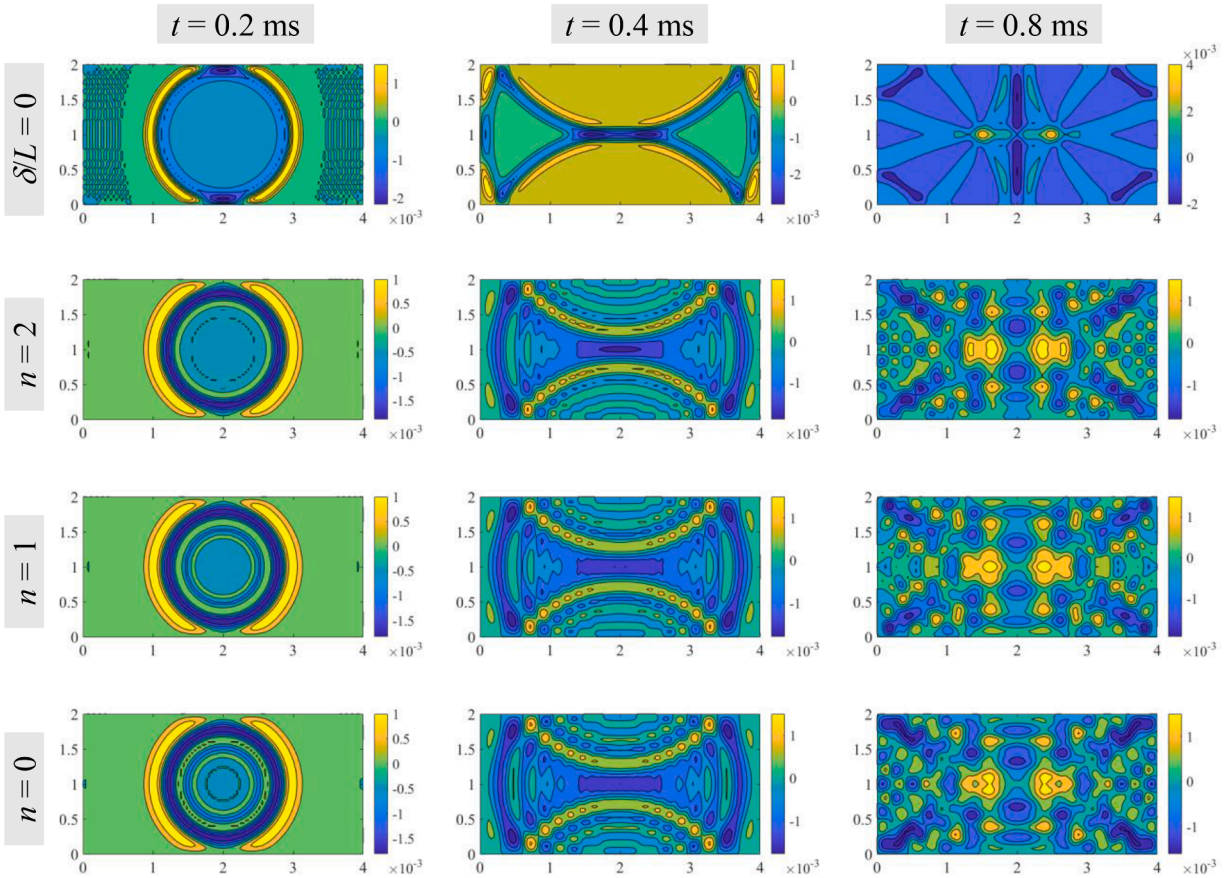

Fig. 14. Example 5: displacement profiles at times $t = 0.2$, 0.4 and 0.8 ms, obtained from the classical solution, and PD solutions with horizon size $0.05H$ for different kernels.

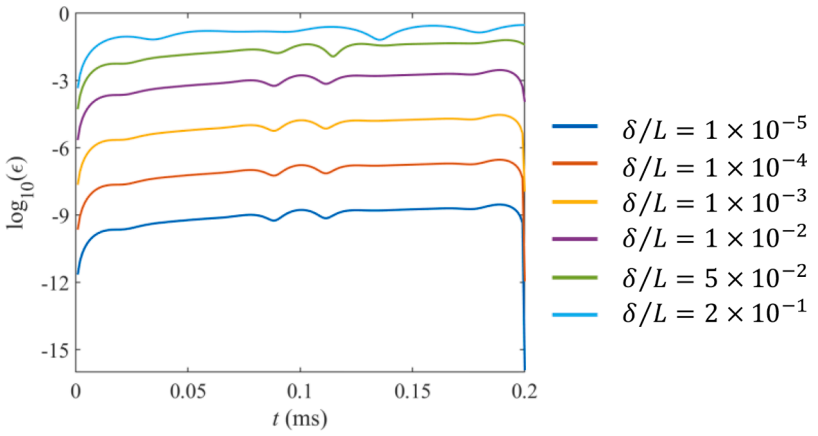

Fig. 15. The evolution of average difference (logarithm scale in the vertical axis) between peridynamic solution and the classical solution, for the case with smooth initial condition (see Section 3.2).

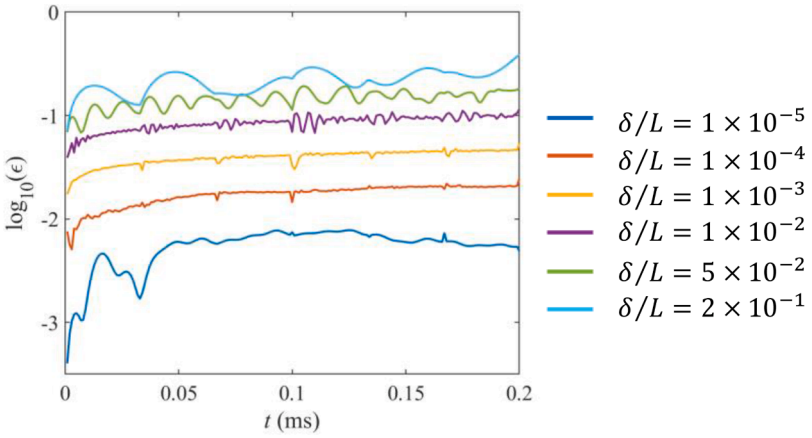

Fig. 16. The evolution of average difference (logarithm scale used in the vertical axis) between peridynamic solution and the classical solution, for the case with jump discontinuity in initial condition (see Section 3.4).

$$u(x,y,t) = \sum_{m=1.3.5\ldots}^{\infty}\sum_{s=1,3,5\ldots}^{\infty} B_{ms}\cos\left(\lambda_{ms}\sqrt{A_n(r)}\,t\right)\sin(k_m x)\sin(k_s y) \tag{54}$$

where, $k_m = \frac{m\pi}{L}$, $k_s = \frac{s\pi}{H}$, $\lambda_{ms} = v\sqrt{{k_m}^2 + {k_s}^2}$, $A_n(r)$ is given in Eq. (49), and,

$$B_{ms} = \frac{4}{LH}\int_0^H\int_0^L u(x,y,0)\sin(k_m x)\sin(k_s y)\mathrm{d}x\mathrm{d}y = \frac{2048}{5m^3s^3\pi^6} \tag{55}$$

The classical solution (recovered for $\delta = 0$) and the PD solutions ($\delta = 0.5H$) at three time snapshots ($t = 0.01$, 0.36, and 0.7 ms) are presented in Fig. 12. The first 101×51 terms of the 2D PD series solutions are used for the plots and videos in Sections 5.2 and 5.3. All of the PD solutions are close to the corresponding classical solutions. In Fig. 13, we show the effect the horizon size has on the membrane vibrations. Only the PD formulation with $n = 2$ is considered for this figure. Three horizon sizes, $0.005H$, $0.1H$ and $0.5H$, are used. Due to the wave dispersion effect, the displacement difference profiles have a different character compared to those noticed from the 2D diffusion case shown in (Chen et al., 2022). Fig. 13 also reveals that the nonlocal effect decreases with the horizon size decreasing, but increases in time, for a fixed horizon size.

The differences between the PD solutions and the corresponding classical solutions are small because the initial displacement field has a large wave-length, relative to the horizon size. In the next section, we study the behavior of a PD solution for the same membrane problem but with an initial condition of a sharp (wave-length in the order of the horizon size) solitary wave.

5.3. *Example 5: solution for a 2D wave propagation problem with Dirichlet boundary conditions*

We consider the same rectangular membrane used in the Example 4, but instead of the whole membrane vibration, in this section we consider the propagation of a sharp solitary wave, with zero initial velocity ($u_t(x,y,0) = 0$) and the initial displacement: $u(x,y,0) = 0.02\exp(-100((x-2)^2 + (y-1)^2))$. The analytical PD solution has the form given in Eq. (54):

$$u(x,y,t) = \sum_{m=1.3.5\ldots}^{\infty}\sum_{s=1,3,5\ldots}^{\infty} B_{ms}\cos\left(\lambda_{ms}\sqrt{A_n(r)}\,t\right)\sin(k_m x)\sin(k_s y) \tag{56}$$

while B_{ms} are:

$$B_{ms} = \frac{0.0008\pi}{LH}\sin\left(\frac{m\pi}{2}\right)\sin\left(\frac{s\pi}{2}\right)\exp\left(-\frac{{k_m}^2 + {k_s}^2}{400}\right) \tag{57}$$

The classical solutions ($\delta = 0$) and PD solutions ($\delta = 0.05H$) at three times ($t = 0.2$, 0.4, and 0.8 ms) are shown in Fig. 14. Even with a horizon size one-tenth of the one used in Fig. 12, the wave dispersion are obvious for the wave propagation shown in Fig. 14.

To see the effect the horizon size has on the complex nonlocal wave dispersion, in Videos 7–10, we present the displacement time-evolution from PD solutions with $n = 2$. Four horizon sizes, $0.005H$, $0.1H$, $0.2H$ and $0.5H$, are used for the results shown in Videos 7–10, respectively. The scalar bar is not given in these videos. Since we aim to analyze the effect of horizon size on the nonlocal wave dispersion, we focus on the displacement contrast and the absolute value at each location is secondary. When horizon size is $0.005H$, Video 7 shows that little dispersion is observed and the membrane deflection profiles are similar to the classical solution shown in Fig. 14. When the horizon size is $0.5H$ (Video 10), the boundary is in the horizon range of the initial location of the wave peak, thus the

behavior of the wave propagation for this horizon size is quite different from the other three cases with smaller horizons.

6. Concluding remarks

In this paper we showed how to use separation of variables to obtain analytical solutions for peridynamic (PD) equations of elastodynamics (1D and 2D) set in simple domains, for which analytical series solutions of the corresponding classical formulation of the same problem exist. We discussed how problems with Dirichlet boundary conditions can be treated. Given a problem for which the classical series solution is available, one can obtain the analytical solution for the corresponding PD problem by simply inserting a nonlocal factor, named here the "peridynamic-" or the "nonlocal factor", in the time-dependent term of the local solution. The nonlocal factors depend on the horizon size and converge to value one as the horizon size goes to zero, recovering the classical form of the solution for the corresponding partial-differential equations.

We computed analytical solutions for several PD example problems with Dirichlet boundary conditions and smooth and discontinuous initial conditions in 1D elastic wave propagation. We also studied elastic vibration and sharp solitary wave propagation in 2D membranes. We showed that the nonlocality in peridynamic elasticity can create complex behavior, induced by nonlocal wave dispersion, and even lead to "random"-like motion. As time goes to infinity, the nonlocal solution did not converge to the classical one for a fixed horizon size, in contrast with the case for diffusion problems, as the effect of nonlocality persists in time. Surprisingly, for problems with discontinuous initial conditions, persistence of discontinuities happens in space as well. The analytical peridynamic solutions derived here and their relationships with the corresponding classical solutions are useful in peridynamic modeling such as selecting the appropriate horizon size, verifying computational methods for approximating PD solutions, etc.

Declaration of Competing Interest

The authors declare that they have no known competing financial interests or personal relationships that could have appeared to influence the work reported in this paper.

Acknowledgements

Z.C. and X.P. were supported by the National Natural Science Foundation of China (No. 11802098). The work of S.J. and F.B was supported in part by the National Science Foundation under CMMI CDS&E award No. 1953346.

Supplementary materials

Supplementary material associated with this article can be found, in the online version, at doi:10.1016/j.ijengsci.2023.103866.

Appendix A: Separation of variables for classical wave equation

In this appendix, we briefly discuss the method of separation of variables for finding solutions to classical wave IBVPs, based on the textbook (Greenberg, 1988).

In one-dimension

The 1D linear classical wave equation is:

$$\frac{\partial^2 u(x,t)}{\partial t^2} = v^2 \nabla^2 u(x,t) \tag{A.1}$$

We assume a solution in the form of the product $u(x,t) = X(x)\mathrm{T}(t)$ and substitute in (A.1):

$$\mathrm{X}(x)\mathrm{T}''(t) = D\mathrm{T}(t)\mathrm{X}''(x) \tag{A.2}$$

where the single and double primes denote the first and the second order ordinary differentiation. Diving (A.2) by XT leads to:

$$\frac{1}{v^2}\frac{\mathrm{T}''(t)}{\mathrm{T}(t)} = \frac{\mathrm{X}''(x)}{\mathrm{X}(x)} \tag{A.3}$$

Since the left hand side of (A.3) is a function of t only, and the right hand side is a function of x only, we conclude that:

$$\frac{1}{v^2}\frac{\mathrm{T}''(t)}{\mathrm{T}(t)} = \frac{\mathrm{X}''(x)}{\mathrm{X}(x)} = \text{constant} = -k^2 \tag{A.4}$$

The negative sign in the constant comes from the fact that a positive sign leads to an unreasonable form for the solution.

According to (A.4), a solution for the partial differential equation (A.1) must be a solution to the following pair of the ordinary differential equations (ODE):

$$\mathrm{T}''(t) + v^2k^2\mathrm{T}(t) = 0 \tag{A.5}$$

$$\mathrm{X}''(x) + k^2\mathrm{X}(x) = 0 \tag{A.6}$$

The general solution for the ODEs are:

$$\mathrm{T}(t) = \begin{cases} Dt + E & k = 0 \\ K\sin vkt + L\cos vkt & k \neq 0 \end{cases} \tag{A.7}$$

$$\mathrm{X}(x) = \begin{cases} Gx + H & k = 0 \\ I\sin kx + J\cos kx & k \neq 0 \end{cases} \tag{A.8}$$

where $D, E, F, G, H, I, J, K, L$ and k are constants to be determined. We then write the formal solution as the superposition of these cases:

$$u(x,t) = \mathrm{XT}|_{k=0} + \mathrm{XT}|_{k\neq 0} = (Gx + H)(Dt + E) + (I\sin kx + J\cos kx)(K\sin vkt + L\cos vkt) \tag{A.9}$$

Constants are determined from initial and boundary conditions for any specific IBVP.

Substituting BCs in (A.9) usually determines all possible numbers for k, and some of the other constants. Then the solution is expressed as the superposition for all possible k's. Finally, the initial condition gives the remaining constants (see (Greenberg, 1988) for examples).

In two-dimensions

The 2D linear classical wave equation is:

$$\frac{\partial^2 u(x,y,t)}{\partial t^2} = v^2\nabla^2 u(x,y,t) \tag{A.10}$$

We assume a solution in the form of the product $u(x,t) = X(x)\mathrm{Y}(y)\mathrm{T}(t)$ and substitute in (A.10) to obtain:

$$\mathrm{X}(x)\mathrm{T}''(t) = v^2\mathrm{T}(t)[\mathrm{X}''(x) + \mathrm{Y}''(y)] \tag{A.11}$$

Division by XYT leads to:

$$\frac{1}{v^2}\frac{\mathrm{T}''(t)}{\mathrm{T}(t)} = \frac{\mathrm{X}''(x)}{\mathrm{X}(x)} + \frac{\mathrm{Y}''(y)}{\mathrm{Y}(y)} = \text{constant} = \psi = -\left(k_1^2 + k_2^2\right) \tag{A.12}$$

and,

$$\frac{\mathrm{X}''(x)}{\mathrm{X}(x)} = -\frac{\mathrm{Y}''(y)}{\mathrm{Y}(y)} - \left(k_1^2 + k_2^2\right) = \text{constant} = \varphi = -k_1^2 \tag{A.13}$$

Similar to the 1D case the negative signs for the constants are used since the positive signs lead to unphysical solution forms. (A.12) and (A.13) gives the three ODEs:

$$\mathrm{T}''(t) + v^2\left(k_1^2 + k_2^2\right)\mathrm{T}(t) = 0 \tag{A.14}$$

$$\mathrm{X}''(x) + k_1^2\mathrm{X}(x) = 0 \tag{A.15}$$

$$\mathrm{Y}''(y) + k_2^2\mathrm{Y}(y) = 0 \tag{A.16}$$

and the general solution for these ODEs are:

$$\mathrm{T}(t) = \begin{cases} Dt + E & \psi = 0 \\ K\sin v\sqrt{-\psi}t + L\cos v\sqrt{-\psi}t & \psi \neq 0 \end{cases} \tag{A.17}$$

$$\mathrm{X}(x) = \begin{cases} Gx + H & k_1 = 0 \\ I\sin k_1 x + J\cos k_1 x & k_1 \neq 0 \end{cases} \tag{A.18}$$

$$\mathrm{Y}(y) = \begin{cases} My + N & k_2 = 0 \\ P\sin k_2 y + Q\cos k_2 y & k_2 \neq 0 \end{cases} \tag{A.19}$$

where $D, E, F, G, H, I, J, K, L$, and k are constants to be determined. We then write the formal solution as the superposition of all possible ψ values:

$$u(x,y,t) = \mathrm{XYT}|_{\psi=0} + \mathrm{XYT}|_{\psi\neq 0} = \mathrm{XYT}|_{k_1=0,k_2=0} + \mathrm{XYT}|_{k_1=0,k_2\neq 0} + \mathrm{XYT}|_{k_1\neq 0,k_2=0} + \mathrm{XYT}|_{k_1\neq 0,k_2\neq 0} \tag{A.20}$$

Similar to the 1D case, k_1, k_2 and other constants are determined from the initial and boundary conditions for any specific IBVP.

Appendix B: Average difference between the PD and classical solutions

To quantitatively investigate the convergence of PD solutions to the corresponding classical solutions, we calculate the average difference for nodes along the bar, in time, between the PD solutions (obtained for several horizon sizes) and the classical solution:

$$\epsilon = \sqrt{\frac{\sum_{i=1}^{N}\left(u_{pd}(t,x_i) - u_c(t,x_i)\right)^2}{N\max\left(u_c\right)^2}} \tag{B.1}$$

where x_i is the coordinate of a set of discrete locations where we make the comparison, N is the total number of nodes used in the comparison (selected here to be equal to 1001), and $u_{pd}(t,x_i)$ and $u_c(t,x_i)$ are the displacements computed from Eqs. (27) and (29) for a finite (nonlocal) and zero (local/classical) horizon sizes, at time t and node x_i, respectively.

Figs. 15 (corresponding to the example in Section 3.2, with smooth initial conditions) and 16 (corresponding to the example in Section 3.4, with discontinuous initial condition) show the evolution of the average difference between the PD and the corresponding classical solutions for different horizon sizes, in time. These figures indicate that in both cases (with or without initial displacement discontinuity) the average difference between the PD solutions and the classical solutions decreases when decreasing the horizon size, meaning that the PD solutions converge to the classical solutions, as expected. Notice that the difference between the PD and classical results is much larger when initial conditions have discontinuities, compared with the case of smooth initial conditions. This is due to the fact that nonlocal models have dispersive properties compared with local operators, and the "infinite number of frequencies packed" into a sharp discontinuity of the initial condition. Further studies on how such discontinuities travel in nonlocal models of dynamic elasticity are warranted and will be the focus of future research.

References

Bobaru, F., & Duangpanya, M. (2012). A peridynamic formulation for transient heat conduction in bodies with evolving discontinuities. *Journal of Computational Physics, 231*, 2764–2785.

Bobaru, F., Yang, M. J., Alves, L. F., Silling, S. A., Askari, E., & Xu, J. F. (2009). Convergence, adaptive refinement, and scaling in 1D peridynamics. *International Journal for Numerical Methods in Engineering, 77*, 852–877.

Chen, J., Tian, Y., & Cui, X. (2018). Free and forced vibration analysis of peridynamic finite bar. *International Journal of Applied Mechanics, 10*, Article 1850003.

Chen, Z., Peng, X., Jafarzadeh, S., & Bobaru, F. (2022). Analytical solutions of peridynamic equations. Part I: transient heat diffusion. *Journal of Peridynamics and Nonlocal Modeling, 4*(3), 303–335.

Chen, Z. G., Bakenhus, D., & Bobaru, F. (2016). A constructive peridynamic kernel for elasticity. *Computer Methods in Applied M, 311*, 356–373.

Chen, Z. G., & Bobaru, F. (2015). Selecting the kernel in a peridynamic formulation: A study for transient heat diffusion. *Computer Physics Communications, 197*, 51–60.

Greenberg, M. D. (1988). *Advanced engineering mathematics*. Prentice-Hall.

Kreyszig, E. (2017). *Advanced engineering mathematics*. John Wiley & Sons.

Lizama, C., Murillo-Arcila, M., & Peris, A. (2020). Nonlocal operators are chaotic. *Chaos (Woodbury, N.Y.), 30*, Article 103126.

Mikata, Y. (2012). Analytical solutions of peristatic and peridynamic problems for a 1D infinite rod. *International Journal of Solids and Structures, 49*, 2887–2897.

Seleson, P. (2014). Improved one-point quadrature algorithms for two-dimensional peridynamic models based on analytical calculations. *Computer Methods in Applied M, 282*, 184–217.

Silling, S. A. (2000). Reformulation of elasticity theory for discontinuities and long-range forces. *Journal of the Mechanics and Physics of Solids, 48*, 175–209.

Silling, S. A. (2016). Solitary waves in a peridynamic elastic solid. *Journal of the Mechanics and Physics of Solids, 96*, 121–132.

Silling, S. A., & Askari, E. (2005). A meshfree method based on the peridynamic model of solid mechanics. *Computers & Structures, 83*, 1526–1535.

Silling, S. A., & Lehoucq, R. B. (2008). Convergence of peridynamics to classical elasticity theory. *Journal of Elasticity, 93*, 13–37.

Silling, S. A., Zimmermann, M., & Abeyaratne, R. (2003). Deformation of a peridynamic bar. *Journal of Elasticity, 73*, 173–190.

Tamm, K., Peets, T., Engelbrecht, J., & Kartofelev, D. (2017). Negative group velocity in solids. *Wave Motion (North-Holland Publishing Company), 71*, 127–138.

Wang, L. J., & Abeyaratne, R. (2018). A one-dimensional peridynamic model of defect propagation and its relation to certain other continuum models. *Journal of the Mechanics and Physics of Solids, 116*, 334–349.

Wang, L. J., Xu, J. F., & Wang, J. X. (2017). Static and dynamic green's functions in peridynamics. *Journal of Elasticity, 126*, 95–127.

Weckner, O., & Abeyaratne, R. (2005). The effect of long-range forces on the dynamics of a bar. *Journal of the Mechanics and Physics of Solids, 53*, 705–728.